Journal of Materials Chemistry

Cite this: *J. Mater. Chem.*, 2012, **22**, 22510

www.rsc.org/materials

PAPER

Monodispersed ultrathin GdF_3 nanowires: oriented attachment, luminescence, and relaxivity for MRI contrast agents†

Yang Tian,* Hong-Yu Yang, Kai Li and Xue Jin

Received 26th July 2012, Accepted 6th September 2012
DOI: 10.1039/c2jm34987f

A facile solvothermal approach was used to synthesize monodispersed ultrathin GdF_3 nanowires *via* an oriented attachment mechanism. Gadolinium nitrate acted as the Gd source, *n*-octylamine and oleic acid as capping ligands, and *n*-octanol as solvent. The phase and morphology of the nanowires were characterized by powder X-ray diffraction and transmission electron microscopy (TEM), respectively. The good monodispersity enabled the nanowires to form mesocrystals in the solution by assembly. The detailed morphological and structural analyses at different time points were observed by TEM and high-resolution TEM to investigate the process of oriented attachment for monodispersed ultrathin GdF_3 nanowires. The organic capping ligands on the GdF_3 surfaces were analyzed through infrared spectra and X-ray photoelectron spectroscopy. The obtained ultrathin GdF_3 nanowires exhibited good monochromaticity with high colour saturation when they were studied as a luminescent host *via* the doping of Eu^{3+} ions. Moreover, for the first time, the one-dimensional (1D) GdF_3 nanostructure was investigated as an MRI contrast agent after being modified by Pluronic F127, although several 0D GdF_3 nanoparticles have been reported as magnetic resonance imaging (MRI) contrast agents. The results indicate that our GdF_3 nanowires had enhanced relaxivity that can be attributed to their ultrasmall diameter and 1D nanostructure.

Introduction

Over the past decades, considerable attention has been directed toward the shape- and size-controlled synthesis of various inorganic nanocrystals because of their shape- and size-dependent properties.[1] Most of the synthesis methods were based on classical Ostwald ripening and were used extensively to describe and explain the growth of large crystals at the expense of smaller ones, as driven by surface energy reduction.[2] However, recent studies have shown that Ostwald ripening does not adequately describe crystal growth for several systems, especially for the anisotropic growth of one-dimensional (1D) and two-dimensional (2D) nanostructures.

Penn and Banfield presented a new crystal growth mechanism involving the attachment between two or more nanocrystals, followed by the sharing of a common crystallographic orientation and the joining with planar interfaces, which is called oriented attachment (OA).[3] The process and mechanism of OA were recently revealed by real-time transmission electron microscopy (TEM),[4] and the reduction of the surface energy of nanocrystals and the increase in entropy were considered as the driving forces for OA growth. Compared with the classical Ostwald ripening, this OA growth is based on the separation of nucleation and the subsequent growth process, thus providing a deeper understanding of the growth process of nano- and mesocrystals to a certain extent.[5]

The OA mechanism has so far explained the growth process of several 1D and 2D nanostructures, including metals, metal oxides, and metal chalcogenides (S, Se and Te), thereby providing an efficient method for the generation of nanocrystals with unique morphologies and controllable sizes.[6–12] For example, Weller and coworkers reported the 2D OA of PbS nanocrystals into ultrathin single-crystal sheets, with dimensions at the micrometer scale, in the presence of chlorine-containing compounds.[6] Lou and coworkers presented the formation of 1D and 2D assemblies of α-Fe_2O_3 nanoparticles by OA through a simple hydrothermal route.[7] Murray and coworkers synthesized monodispersed PbSe nanorods in a catalyst-free, one-pot reaction by using a new phosphine selenide precursor.[8] Wang and coworkers reported a number of metal-oxide ultrasmall nanowires, such as SnO_2, ZrO_2, and InOOH, by using an OA approach.[9] Li and coworkers prepared V–VI binary and ternary hexagonal platelets in the OA mechanism.[10] Recently, our group reported the OA mechanism in fluoride for the preparation of GdF_3 ultrasmall nanowires *via* a solvothermal method, in which $Gd(acac)_3$ was used as Gd source and *n*-octylamine as capping ligand.[11] Although considerable progress has been achieved in

Department of Chemistry, Capital Normal University, Beijing, P. R. China. E-mail: tianyang@mail.sdu.edu.cn; Fax: +86-10-68903040; Tel: +86-10-68903033

† Electronic supplementary information (ESI) available: Details of characterization including TEM images, FFT, EDX, photographs, and calculations of surface-to-volume ratio for 0D nanoparticles and 1D nanowires. See DOI: 10.1039/c2jm34987f

the OA mechanism, obtaining of aggregation-free monodispersed 1D or 2D nanostructures through OA growth remains a challenge.

Monodispersed nanostructures are pursued because their exposed surfaces can be used in such processes as catalysis, bioconjunction, surface-modification, phase transfer, and so on. Meanwhile, GdF_3 nanostructures have received considerable interest because of their potential applications in biolabels, optical devices, magnetic resonance imaging (MRI), and so on.[13] In this paper, aggregation-free ultrathin GdF_3 nanowires were prepared *via* an OA mechanism similar to our previous report.[11] Aside from the perfect monodispersity, three other advantages are demonstrated in the present work compared with the previous preparation of GdF_3 ultrasmall nanowires: (1) inexpensive $Gd(NO_3)_3$ was applied as Gd source as a substitute for expensive $Gd(acac)_3$; (2) the material showed good monochromatic luminescence with high colour saturation when doped with Eu^{3+}; (3) this study is the first to present the 1D GdF_3 nanostructure as an enhanced MRI contrast agent, although several 0D GdF_3 nanoparticles have been reported as MRI contrast agents previously.[14]

Experimental

Synthesis of monodisperse GdF_3 and GdF_3:Eu^{3+} ultrathin nanowires

All the reagents were analytical grade and used without further purification. In a typical synthesis of GdF_3 nanowires, $Gd(NO_3)_3 \cdot XH_2O$ (0.3 mmol, $X = 5$–6, ACROS) was dissolved into octylamine (3.0 ml, ACROS), octanol (10.0 ml, Tianjin Reagents Inc.) and oleic acid (1.0 ml, Tianjin Reagents Inc.) under agitation for 10 min at room temperature. After formation of a homogeneous solution, it was transformed into a Teflon bottle (20 ml), and then 60 μml HF (Tianjin Reagents Inc.) was added into the mixture. The Teflon bottle was sealed in a stainless autoclave and put into an oven at 240 °C for 1 h. After cooling to the ambient temperature, white precipitates at the bottom were separated by centrifugation with a speed of 5000 rpm, and washed by ethanol. The obtained precipitate could be well-dispersed in nonpolar solvents such as chloroform and cyclohexane. The GdF_3 nanowires doped with Eu^{3+} (5 mol%, 10 mol %, and 20 mol%) could be prepared *via* a similar method by stoichiometric $Eu(NO_3)_3 \cdot XH_2O$ (X = 5–6) substituting $Gd(NO_3)_3 \cdot XH_2O$ ($X = 5$–6) in the precursor solution.

Transfer of the prepared GdF_3 ultrathin nanowires from a nonpolar solvent to water

This process was performed based on ref. 15. In brief, a concentrated suspension of as-synthesized GdF_3 nanowires dispersed in hexane was mixed with an aqueous solution containing an appropriate amount of Pluronic F127 (PF127) followed by vigorous agitation for 30 min. The obtained solution was heated at *ca.* 80 °C to remove the hexane in the solution.

Characterization

Powder X-ray diffraction (XRD) patterns were collected on a Rigaku D/Max 2200 PC diffractometer with CuKα radiation ($\lambda = 1.5418$ Å) and graphite monochromator from 20 to 70° at a scanning rate 5° per min. The particle size and morphology of the resulting nanoparticles were characterized on a transmission electron microscopy (TEM, JEM100-CXII) equipped with selected area electron diffraction (SAED). The structure of nanocrystals was observed by HRTEM (GEOL-2010). Infrared spectrum (Nicolet 5DX FT-IR instrument, KBr pellet technique) and X-ray photoelectron spectroscopy (XPS) analyses were applied to characterize the nanocrystals' surface. The XPS spectra were recorded on a PHI-5300 ESCA spectrometer (Perkin–Elmer) with its energy analyzer working in the pass energy mode at 35.75 eV, and the AlKα line was used as excitation source. After subtraction of X-ray satellites and inelastic background (Shirley-type), peak deconvolution was carried out. Full width at half maximum (FWHM) was kept the same for chemical components within the same core level of an element, and all component peaks were set to be Gaussian-type. The chemical composition of the as-prepared nanowires doped with Eu^{3+} was analyzed by energy dispersive X-ray spectroscopy (EDX, Oxford). The fluorescence properties of all the samples were investigated under an Edinburgh lifetime and steady state spectrometer (FLS920) equipped with 450 W Xe lamps. The samples for fluorescence testing were prepared by obtaining solid powders of the samples. The Gd^{3+} concentration in the aqueous solution was analyzed using inductively coupled plasma mass spectrometry (ICP-MS, Agilent 7500C). The relaxation time T_1 and T_1-weighted images were measured at 7.0 T by proton Larmor frequency (Varian 7.0 T/160 mm small animal research MRI scanner).

Results and discussion

Fig. 1 shows the powder X-ray diffraction (XRD) pattern of the obtained GdF_3 nanowires from 20° to 70°. Nearly all the diffraction peaks are in good agreement with the previously reported crystalline GdF_3 (JCPDS Card 49-1804), illustrating their orthorhombic structure (inset of Fig. 1) and few impurities. The morphology and size of the as-prepared GdF_3 nanowires were characterized by TEM, as shown in Fig. 2a. The figure shows that the GdF_3 ultrathin nanowires are nearly monodispersed, with diameters of *ca.* 2 nm and lengths of 20 nm to

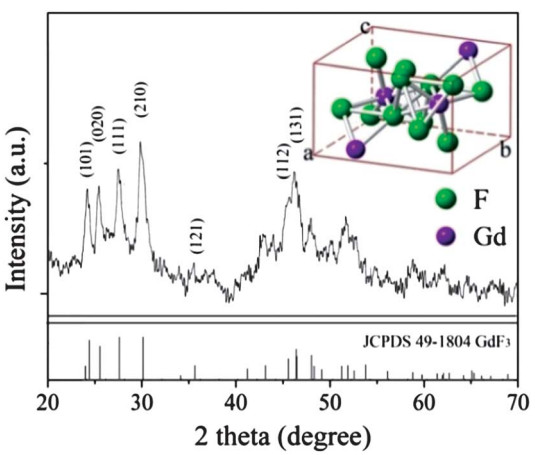

Fig. 1 XRD pattern and crystalline structure (inset) of the obtained GdF_3 sample.

40 nm. Interestingly, although the crystalline nanowires look flexible as most of them bend on the film, they do not aggregate. The selected area electron diffraction (SAED, inset of Fig. 2a) for the sample illustrates the crystalline nature of the nanowires. The line spacing of the GdF_3 ultrathin nanowires is approximately 4 nm, which is in accordance with the double length of the oleic acid molecule (1.7 nm to 2.4 nm).[6] The ultrathin nanowires are also shown to possess a rough surface, high densities of defects, and evident small building blocks in the 1D direction. All these characteristics demonstrate that the structure of GdF_3 nanowires was achieved by the OA mechanism. Interestingly, some GdF_3 nanowires in the solution can bring a liquid-crystalline assembly to generate short belt-like mesocrystals, as shown in Fig. 2b. The microstructure of the mesocrystals was characterized by high-resolution TEM (HRTEM), as shown in the inset of Fig. 2b, whereby the line spacing of nanowires is approximately 2.5 nm, which is in accordance with the double length of octylamine molecule or the single length of the oleic acid molecule. These mesocrystals can be further confirmed by prolonging the reaction time to 24 h to yield the GdF_3 nanocrystals with the shape and size similar to the mesocrystals (see the ESI, Fig. S1†).[16]

The detailed morphological and structural analysis at different time points during the reaction was observed by TEM and HRTEM to further investigate the OA process of ultrathin GdF_3 nanowires. In the first 5 min of the reaction, small particles with sizes of *ca.* 2 nm were produced from the reaction between the gadolinium and fluorine precursors, as shown in Fig. S2 (see the ESI†). Fig. 3a is the HRTEM image of an individual small particle, showing the crystalline planes with distances of *ca.* 0.32 nm that are assigned to plane {111} of the orthorhombic GdF_3, which is sketched in Fig. 3I. As the reaction continues, the original particles can be recognized along with aggregates, forming short nanowires. Fig. S3 (see the ESI†) is a TEM image of the product obtained after 10 min of the reaction. Short wires with clear building blocks of nanoparticles are observed. Fig. 3b–d identifies this structure as the aggregate of two particles attached in one dimension in three different ways by studying the junctions between the attached particles. The first way, twin-crystal (TC) attachment, implies that crystals on both sides of the junction share one interface. In Fig. 3b, the HRTEM image indicates that one set of {111} planes remained continuous, while the other set of {111} planes are related by a mirror-symmetry across the boundary (sketched in Fig. 3II). The coherent twin boundary, being a low-energy interface, gives rise to this possibility. The fast Fourier transform (FFT) from this region (see the ESI, Fig. S4†) reveals the twin relationship. The second way, interface-defect (ID) attachment, presents that the attached surfaces of the two connected nanocrystals are plane groups with a crystalline defect. In Fig. 3c, the HRTEM image indicates that the {210} planes of the two nanocrystals were connected through an ID attachment, with an angle of *ca.* 22°, and the interface has a high index plane with step defects (sketched in Fig. 3III). The mismatch of interface lattices inevitably introduces lattice distortion and reconstruction. The third way, plane-match (PM) attachment, indicates that two nanocrystals are connected by the extension of the matching two sets of planes to form a single crystal. In Fig. 3d, the HRTEM image demonstrates the

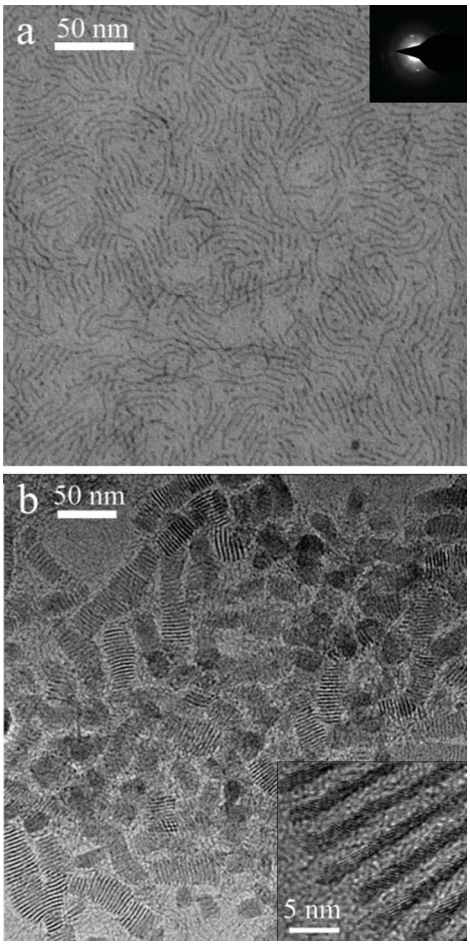

Fig. 2 TEM image of the obtained GdF_3 nanowires (a), the inset is the SAED pattern of the nanowires; TEM image of the mesocrystals of GdF_3 nanowires (b), the inset is the magnification.

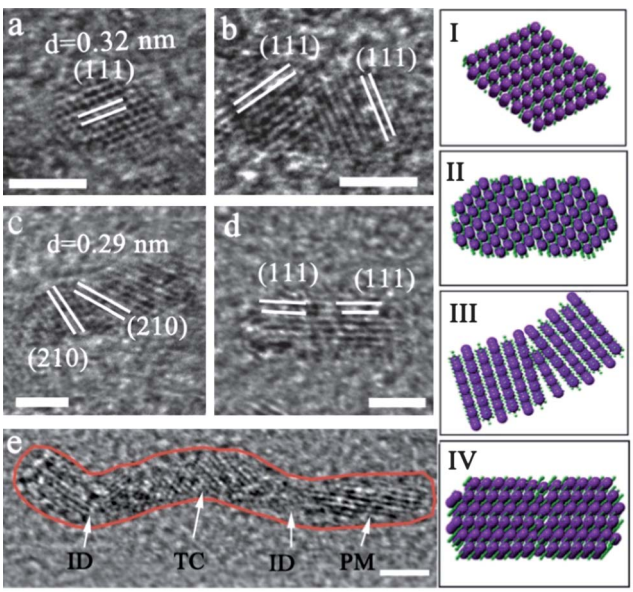

Fig. 3 HRTEM images for GdF_3 samples of the initial nanodots (a), short nanorods attached by two nanocrystals (b–d), and a single nanowire (e). Schematic diagram of the HRTEM images (I–IV). The bars are all 2 nm.

evolution of a rod-like single crystal from the precise oriented attachment of two nanocrystals with two sets of {111} planes that connect and extend through plane matching (sketched in Fig. 3IV). This type of attachment reduces the interface energy by the greatest amount.[9a] Fig. 3e displays the HRTEM of a single GdF_3 nanowire obtained from the reaction for 40 min. All the three attachment types of OA are well illustrated, suggesting that the OA process accounts for the formation of nanowires.

We have reported previously that this oriented attachment is induced by the surface capping ligands anchoring to some specific GdF_3 surfaces selectively, thus facilitating the oriented attachment along the no (or less) capped crystal planes. In this study, the capping ligands on the GdF_3 surfaces are studied in more detail to explain the formation of monodispersed nanowires by the OA mechanism. Fig. 4a displays the TEM image of the obtained GdF_3 product with 4 ml of octylamine in a reaction solution that is free of oleic acids. 1D nanowries with branches and aggregated GdF_3 were obtained, as depicted in our previous report, although $Gd(NO_3)_3$ replaced $Gd(acac)_3$ as the Gd source in this work.[11] This result suggests that octylamine is selectively capping on the planes of GdF_3 nanocrystals and thus plays a key role in the 1D OA. Monodispersed ultrathin nanowires were obtained when 3 ml of octylamine and 1 ml of oleic acid were added to the reaction solution, as shown in Fig. 2. This finding shows that a spot of oleic acid is also selective to GdF_3 surfaces because they have a preferential removal from the planes to solution. However, when 4 ml of oleic acid was added to a reaction solution free of octylamine, the obtained GdF_3 sample tends to be polydispersed nanoparticles rather than nanowires, which are approximately 10 nm in size (Fig. 4b). Fewer nuclei are formed when a large excess of oleic acid is present, thus resulting in polydispersed larger nanoparticles.[17] This result indicates that excess oleic acid in the solution is inclined to cap the surfaces of nanoparticles, thereby interrupting OA of the nanoparticles. The results also illustrate that the size of the nanoseeds plays a crucial role in determining the morphology evolution of nanoseeds for OA, as reported previously.[7,9d] Only when the size of nanoparticles is small enough can the 1D OA process be detected. The big size of GdF_3 nanoparticles obtained with excess oleic acid (Fig. 4b) was another factor in interrupting the OA of the nanoparticles. Therefore, although octylamine can facilitate OA growth of GdF_3 along the 1D direction, an appropriate amount of oleic acid is essential for the monodispersity of the nanowires. The reasonable effects of octylamine and oleic acid on OA and monodispersed nanowires are shown in Fig. 4c.

The surface of monodispersed GdF_3 nanowires was also studied by using Fourier-transform infrared spectroscopy (FT-IR) and X-ray photoelectron spectrometry (XPS) analyses. Fig. 5a shows the FT-IR spectrum of the sample. The broad band at *ca.* 3400 cm^{-1} was assigned to the stretching vibrations of N–H bonds and the adsorbed water molecules, and the absorptions at *ca.* 2900 cm^{-1} correspond to the stretching vibrations of C–H bonds. Peaks at *ca.* 1540 and 1468 cm^{-1} are also found in the spectrum and are associated with the asymmetric and symmetric stretching vibrations of the carboxylic group of the bound oleic acid.[18] The peak located at *ca.* 1629 cm^{-1} was assigned to the bending vibrations of N–H bonds. The peak at *ca.* 1162 cm^{-1} arises from the stretching vibrations of C–N bonds. Fig. 5b shows a typical XPS survey spectrum for the sample. The binding energy reference was taken at 284.7 eV for the C1s peak arising from the surface hydrocarbons. The survey spectrum confirms the presence of abundant F and Gd elements, as well as trace O and N elements. The high-resolution XPS pattern for the N element in our sample (Fig. 5c) shows a good symmetrical peak, illustrating that the N in the sample relates to only one chemical environment. The peak located at *ca.* 400.4 eV accounts for the N in the octylamine.[19] Fig. 5d shows the high-resolution XPS pattern for O. The figure shows a small peak located at approximately 532.7 eV coming from the O atoms in –OH and –C═O,[20] indicating traces of physically absorbed oleic acid. A main peak at 531.1 eV can be attributed to the conjugated O atoms in –OH and –C═O of oleic acid capping to the GdF_3

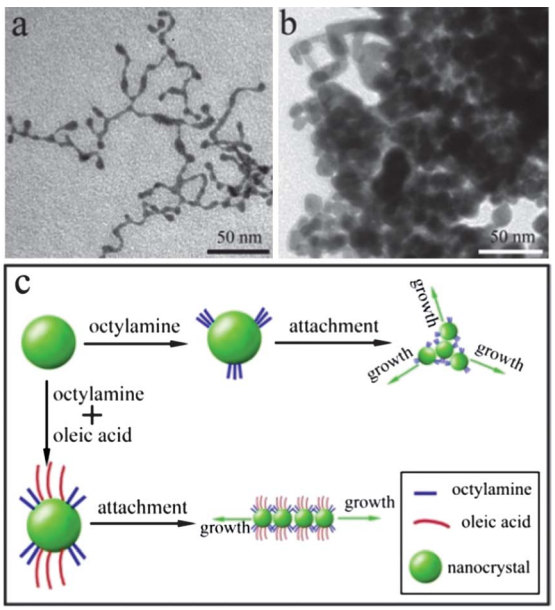

Fig. 4 TEM images of the GdF_3 obtained with 4 ml of octylamine free of oleic acid (a) and with 4 ml of oleic acid free of octylamine (b); schematic diagram of the products with different capping ligands (c).

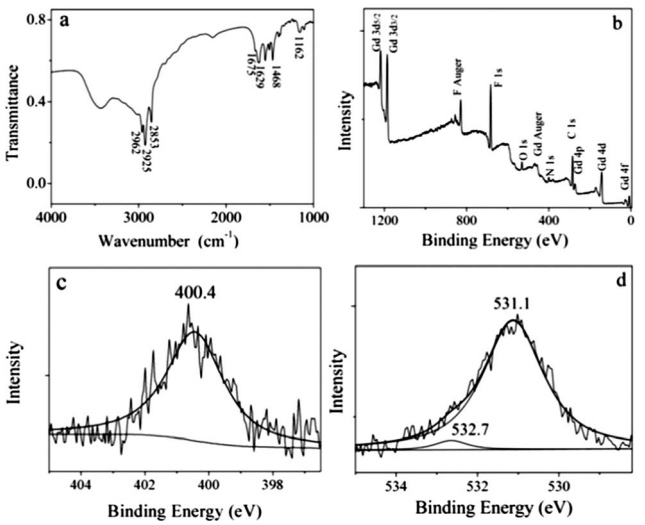

Fig. 5 FT-IR of the ultrathin GdF_3 nanowires (a); XPS for survey spectra (b), N element (c), and O element (d) of the sample.

nanowires because binding energy will shift to a lower value as N or O atoms bound to metals because of a transfer of electron density.[21] These results also indicate that monodispersed nanowires are capped with both oleic acid and octylamine, thus inducing the occurrence of OA growth and perfect monodispersity.

To investigate the luminescence of the obtained GdF_3 ultrathin nanowires, Eu^{3+} ions were doped into nanowires with different concentrations (5 mol%, 10 mol% and 20 mol%) by using the same synthetic pathway (see the ESI, Fig. S5†), which was identified by using energy-dispersive X-ray spectroscopy (EDX, see the ESI, Fig. S6†). Fig. 6a is the excitation spectrum of GdF_3 nanowires doped by 10 mol% Eu^{3+} at room temperature, and it is similar to samples with doping of 5 mol% Eu^{3+} and 20 mol% Eu^{3+}. The excitation spectrum consists of the characteristic absorption peaks of Eu^{3+} corresponding to the direct excitation from the europium ground state into the higher excited states of the europium f-electrons. The position of these sharp lines is practically identical to the characteristic absorption for the transition in Eu^{3+} and the excitation spectra reported for other Eu^{3+}-doped materials.[22] In addition, the charge-transfer (CT) band of Eu^{3+}-F^- is absent at approximately 240 nm in the excitation spectrum, as expected. In Eu^{3+}-doped systems, CT occurs *via* electron delocalization from the filled 2p shell of the ligand to the partially filled 4f shell of Eu^{3+}.[22,23] The transition energy depends strongly on the electronegativity of the ligand. Given the high electronegativity of pure fluoride systems, a significantly larger amount of energy is needed to remove an electron from F^-. Thus, the CT band in the excitation spectrum is located below 200 nm, which differs from conventional Eu-doped oxide phosphors.[24]

Fig. 6b shows the emission spectra for the GdF_3 ultrathin nanowires with different Eu^{3+} concentrations (5 mol%, 10 mol% and 20 mol%) excited by a 397 nm wavelength at room temperature. The spectra show that the samples have characteristic emission peaks of Eu^{3+} within the range of 500 nm to 750 nm, corresponding to the $^5D_0 \rightarrow {}^7F_J$ line transitions ($J = 0$, 1, 2, 3, 4) of Eu^{3+}. The 4f energy levels of Eu^{3+} are hardly affected by the crystal field because of the shielding of the $5s^25p^6$ electrons. Therefore, no notable shift in the positions of the emission peaks were observed in our ultrathin nanowires compared with other Eu^{3+}-doped systems.[22,23] The figure shows that the GdF_3 with the doping of 10 mol% Eu^{3+} emits the highest intensity in the three samples with a quantum yield (QY) of 20.78%. The QYs for samples with 5 mol% and 20 mol% Eu^{3+} are 9.52% and 17.31%, respectively. Meanwhile, the intensity of the magnetic-dipole-allowed $^5D_0 \rightarrow {}^7F_1$ transition (590 nm) exceeds that of the electron-dipole-allowed $^5D_0 \rightarrow {}^7F_2$ transition (612 and 617 nm) in the three emission spectra, indicating the good monochromaticity and the inversion symmetry of the Eu^{3+} site in the ultrathin nanowires.[25] The luminescent dynamics of the three samples were also measured at room temperature. As shown in the inset of Fig. 6b, decay curves of the three samples corresponding to the $^5D_0$ level of Eu^{3+} in the ultrathin nanowires are the biexponential decay, illustrating that the decay time arises from two kinds of luminescent centers, namely, the Eu^{3+} ions on the surface and in the inner side. The values of average decay time for the samples are calculated respectively as 3.86 ms (5 mol%), 3.28 ms (10 mol%), and 3.23 ms (20 mol%), based on the decay components (see the ESI, Table S1†).

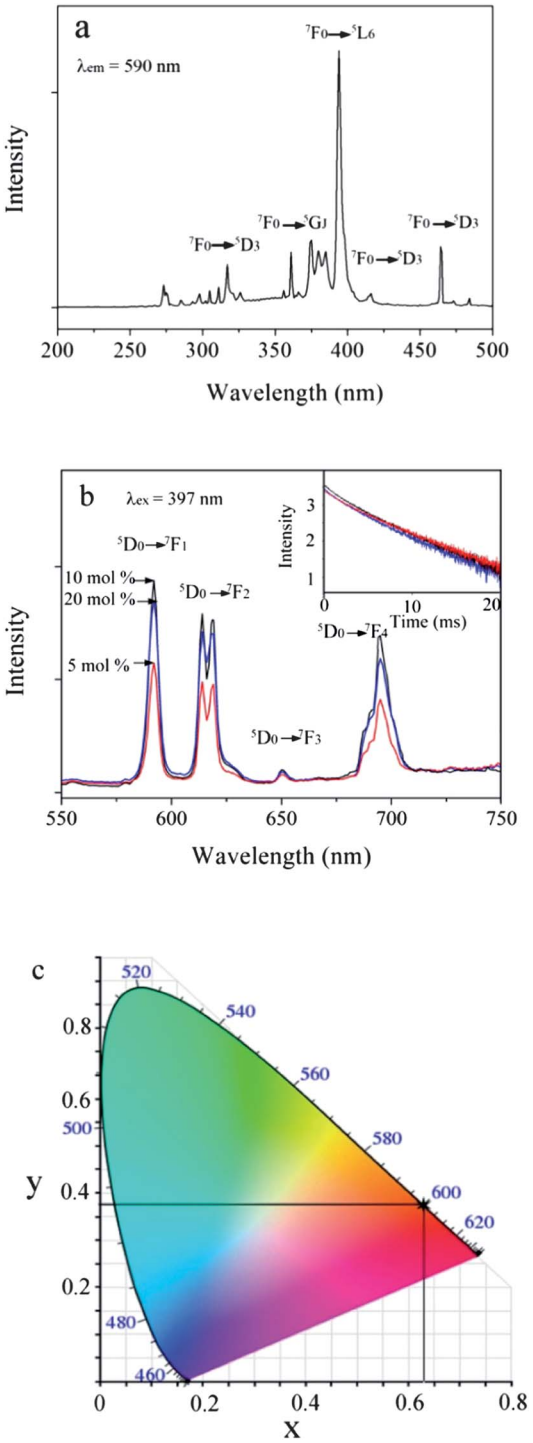

Fig. 6 Excitation spectrum (a) of the GdF_3 nanowires with doping of 10 mol% Eu^{3+}; emission spectra (b) of the GdF_3 nanowires with doping of 5 mol% (red line), 10 mol% (blue line) and 20 mol% (black line) Eu^{3+}, as well as their decay curves (inset); CIE chromaticity diagram for the three samples (c).

Fig. 6c is the corresponding International Commission on Illumination (CIE) chromaticity diagram for the emission spectra of the Eu^{3+}-doped GdF_3 ultrathin nanowires (5 mol%, 10 mol% and 20 mol%). The figure displays that the CIE

coordinates for the three samples locate at the same position nearly, where $x = 0.626$ and $y = 0.374$ (5 mol%), $x = 0.624$ and $y = 0.376$ (10 mol%), as well as $x = 0.629$ and $y = 0.371$ (20 mol %). Moreover, they are just on the outer curved boundary with red–orange colour. The chromaticity diagram is a tool to specify how the human eye will experience light at a given spectrum. The outer curved boundary is called the spectral locus, which corresponds to monochromatic light with wavelengths listed in nanometers. More saturated colours appear closer to the outer curve boundary in the CIE chromaticity diagram.[26] Therefore, the emission of our Eu^{3+}-doped ultrathin GdF_3 nanowires exhibits good monochromatic light with high colour saturation, which refers to how vivid and intense a colour is.

Nanoparticles based on Gd^{3+} are well known to show tremendous potential as T_1 contrast agents for MRI.[27] The efficiency of a contrast agent is usually expressed as its relaxivity r_1 or r_2, that is, the rates of proton relaxation of longitudinal and transverse processes, respectively. T_1 contrast agents are preferred over T_2 agents because the enhanced brightening effect of the former can easily be used to differentiate the signal from other pathogenic or biological conditions.[17,27b] To investigate the relaxation efficiency of MRI contrast agents, the as-prepared 1D monodispersed GdF_3 nanowires were redissolved in a hyperpure water solution after modification with the surfactant Pluronic F127 according to the literature (see the ESI, Fig. S7†).[15] The Gd^{3+} concentration in the solution was determined by using inductively coupled plasma mass spectrometry (ICP-MS). Solutions with different Gd^{3+} concentrations diluted by hyperpure water were then measured at 7.0 T at room temperature. Fig. 7a shows the relaxation rates $1/T_1$ as a function of the Gd^{3+} concentration for the nanowires, in which T_1 relaxation processes result from the interaction between the excited nuclei and their surrounding environment. The r_1 is approximately 15.0 s^{-1} mM^{-1} from the slope of the plot of $1/T_1$ *versus* the Gd^{3+} concentration. The r_1 value of 15.0 s^{-1} mM^{-1} at 7.0 T for our ultrathin nanowires is even higher than the value of 14.3 s^{-1} mM^{-1} for GdF_3 nanoparticles reported previously, which was measured at a higher magnetic field (14.1 T).[13a] Fig. 7b represents T_1-weighted magnetic resonance images for the solutions of GdF_3 ultrathin nanowires, demonstrating a positive enhancement of the effect on T_1-weighted sequences as the nanowire concentration increases. Therefore, the prepared GdF_3 ultrathin nanowires are considered as a potential MRI contrast agent with good performance.

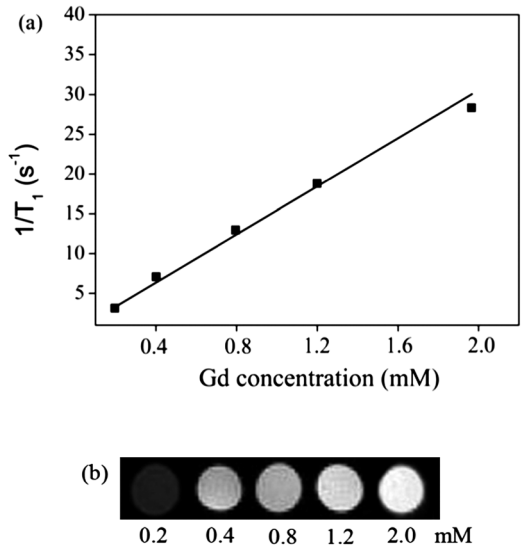

Fig. 7 Relaxivity (a) and T_1-weighted images with different Gd^{3+} concentrations (b) of GdF_3 ultrathin nanowires at 7.0 T.

It was reported that relaxivity enhancement for nanoparticles depends mainly on surface-to-volume ratio (S/V) and tumbling time (τ_R).[17,28] T_1 contrast agents require immediate contact with water molecules to expedite T_1 relaxation effectively due to the inherent spin-lattice relaxation. The high S/V ratio enables more Gd^{3+} ions residing on the surface to come in contact with the water molecules, thus contributing significantly to the longitudinal relaxation of water protons. The S/V ratio for our ultrathin 1D GdF_3 nanowires, with a diameter of 2 nm, is very high (equal to that of 0D nanoparticles of 3 nm approximately, see the ESI†), thereby inducing the relaxivity enhancement of GdF_3 nanowires. Furthermore, the longer tumbling time (τ_R) of contrast agents results in faster relaxation rates.[17] For 0D nanoparticles, the tumbling time (τ_R) shortens as nanoparticle size decreases, thus counteracting the effect of the S/V ratio. For our obtained GdF_3 nanowires, the large length in 1D direction and the low symmetry of nonspherical structure facilitate their longer tumbling times (τ_R) compared with spherical nanoparticles, thus resulting in the further relaxivity enhancement of our sample. Therefore, the ultrasmall diameter and 1D nanostructure of the ultrathin GdF_3 nanowires are considered to be responsible for the relaxivity enhancement.

Conclusions

In summary, a simple solvothermal approach was employed to prepare aggregation-free ultrathin GdF_3 nanowires *via* an OA mechanism. The TEM characterization indicates that the GdF_3 nanowires were nearly monodispersed, with uniform diameters of *ca.* 2 nm and lengths of 20 nm to 40 nm. The good monodispersity enabled the nanowires to form mesocrystals in the solution by assembly. The surface ligands of octylamine and oleic acid were confirmed to be responsible for the OA and monodispersity. The luminescence of the Eu^{3+}-doped GdF_3 ultrathin nanowires shows good monochromatic light with high colour saturation, which refers to how vivid and intense a colour is. Furthermore, this study is the first to investigate 1D GdF_3 nanostructures as an MRI contrast agent. The results indicated that our ultrathin GdF_3 nanowires exhibited enhanced relaxivity, which can be attributed to their ultrasmall diameter and 1D nanostructure.

Acknowledgements

This study is supported by the Beijing Natural Science Foundation (no. 2103048), Funding Project for Academic Human Resources Development in Institutions of Higher Learning Under the Jurisdiction of Beijing Municipality (PHR20100718), and Beijing Excellent Talent (2010D005016000008).

Notes and references

1 (*a*) A. P. Alivisatos, *Science*, 1996, **271**, 933–937; (*b*) C. B. Murray, C. R. Kagan and M. G. Bawendi, *Annu. Rev. Mater. Sci.*, 2000, **30**, 545–610; (*c*) J. J. Li, Y. A. Wang, W. Z. Guo, J. C. Keay, T. D. Mishima, M. B. Johnson and X. G. Peng, *J. Am. Chem. Soc.*, 2003, **125**, 12567–12575; (*d*) T. Hyeon, S. S. Lee, J. Park, Y. Chung and H. B. Na, *J. Am. Chem. Soc.*, 2001, **123**, 12798–12801; (*e*) X. Wang, J. Zhuang, Q. Peng and Y. D. Li, *Nature*, 2005, **437**, 121–124.

2 I. M. Lifshitz and V. V. Slyozov, *J. Phys. Chem. Solids*, 1961, **19**, 35–50.

3 (*a*) R. L. Penn and J. F. Banfield, *Geochim. Cosmochim. Acta*, 1999, **63**, 1549–1557; (*b*) J. F. Banfield, S. A. Welch, H. Z. Zhang, T. T. Ebert and R. L. Penn, *Science*, 2000, **289**, 751–754.

4 (*a*) D. Li, M. H. Nielsen, J. R. I. Lee, C. Frandsen, J. F. Banfield and J. J. De Yoreo, *Science*, 2012, **336**, 1014–1018; (*b*) H.-G. Liao, L. Cui, S. Whitelam and H. Zheng, *Science*, 2012, **336**, 1011–1014.

5 (*a*) V. M. Yuwono, N. D. Burrows, J. A. Soltis and R. L. Penn, *J. Am. Chem. Soc.*, 2010, **132**, 2163–2165; (*b*) R.-Q. Song and H. Colfen, *Adv. Mater.*, 2010, **22**, 1301–1330; (*c*) J. Fang, B. Ding and H. Gleiter, *Chem. Soc. Rev.*, 2011, **40**, 5347–5360.

6 (*a*) C. Schliehe, B. H. Juarez, M. Pelletier, J. Sander, D. Greshnykh, M. Nagel, A. Meyer, S. Foerster, A. Kornowski, C. Klinke and H. Weller, *Science*, 2010, **329**, 550–553; (*b*) Z. Wang, C. Schliehe, T. Wang, Y. Nagaoka, Y. C. Cao, W. A. Bassett, H. Wu, H. Fan and H. Weller, *J. Am. Chem. Soc.*, 2011, **133**, 14484–14487.

7 J. S. Chen, T. Zhu, C. M. Li and X. W. Lou, *Angew. Chem., Int. Ed.*, 2011, **50**, 650–653.

8 W. Koh, A. C. Bartnik, F. W. Wise and C. B. Murry, *J. Am. Chem. Soc.*, 2010, **132**, 3909–3913.

9 (*a*) X. Xu, J. Zhuang and X. Wang, *J. Am. Chem. Soc.*, 2008, **130**, 12527–12535; (*b*) X. Xu and X. Wang, *Nano Res.*, 2009, **2**, 891–902; (*c*) S. Shen, J. Zhuang, X. Xu, A. Nisar, S. Hu and X. Wang, *Inorg. Chem.*, 2009, **48**, 5117–5128; (*d*) S. Shen and X. Wang, *Chem. Commun.*, 2010, **46**, 6891–6899.

10 G. Zhang, W. Wang, X. Lu and X. Li, *Cryst. Growth Des.*, 2009, **9**, 145–150.

11 Y. Tian, J. Tian, X. Li, B. Yu and T. Shi, *Chem. Commun.*, 2011, **47**, 2847–2849.

12 (*a*) G. Zhu, S. Zhang, Z. Xu, J. Ma and X. Shen, *J. Am. Chem. Soc.*, 2011, **133**, 15605–15612; (*b*) Z. Tang, Z. Zhang, Y. Wang, S. C. Glotzer and N. A. Kotov, *Science*, 2006, **314**, 274–278; (*c*) J. Zheng, F. Huang, S. Yin, Y. Wang, Z. Lin, X. Wu and Y. Zhao, *J. Am. Chem. Soc.*, 2010, **132**, 9528–9530; (*d*) D. G. Stroppa, L. A. Montoro, A. Beltrán, T. G. Conti, R. O. da Silva, J. Andrés, E. R. Leite and A. Ramirez, *Chem. Commun.*, 2011, **47**, 3117–3119; (*e*) Z. Peng, H. You and H. Yang, *ACS Nano*, 2010, **4**, 1501–1510; (*f*) C. O'Sullivan, R. D. Gunning, A. Sanyal, C. A. Barrett, H. G. Geaney, F. R. Laffir, S. Ahmed and K. Ryan, *J. Am. Chem. Soc.*, 2009, **131**, 12250–12257; (*g*) Y. Yang, Y. Jin, H. He and Z. Ye, *CrystEngComm*, 2010, **12**, 2663–2665; (*h*) H. Zhang, J. Huang, X. Zhou and X. Zhong, *Inorg. Chem.*, 2011, **50**, 7729–7734.

13 (*a*) T. Paik, D.-K. Ko, T. R. Gordon, V. Doan-Nguyen and C. B. Murry, *ACS Nano*, 2011, **5**, 8322–8330; (*b*) C. Lorbeer, J. Cybinska and A.-V. Mudring, *Chem. Commun.*, 2010, **46**, 571–573; (*c*) F. N. Sayed, V. Grover, V. Sudarsan, B. N. Pandey, A. Asthana, R. K. Vatsa and A. K. Tyagi, *J. Colloid Interface Sci.*, 2011, **367**, 161–170; (*d*) H.-T. Wong, H. L. W. Chan and J. H. Hao, *Appl. Phys. Lett.*, 2009, **95**, 022512; (*e*) J. Shen, L. Sun and C. Yan, *Dalton Trans.*, 2008, 5687–5697.

14 (*a*) F. Evanics, P. R. Diamente, F. C. J. M. van Veggel, G. J. Stanisz and R. S. Prosser, *Chem. Mater.*, 2006, **18**, 2499–2505; (*b*) Q. Ju, Y. Liu, D. Tu, H. Zhu, R. Li and X. Chen, *Chem.–Eur. J.*, 2011, **17**, 8549–8554.

15 H. Fan, E. Leve, J. Gabaldon, A. Wright, R. E. Haddad and C. J. Brinker, *Adv. Mater.*, 2005, **17**, 2587–2590.

16 V. M. Yuwono, N. D. Burrows, J. A. Soltis and R. L. Penn, *J. Am. Chem. Soc.*, 2010, **132**, 2163–2165.

17 N. J. J. Johnson, W. Oakden, G. J. Stanisz, R. S. Prosser and F. C. J. M. van Veggel, *Chem. Mater.*, 2011, **23**, 3714–3722.

18 Z. Chen, H. Chen, H. Hu, M. Yu, F. Li, Q. Zhang, Z. Zhou, T. Yi and C. Huang, *J. Am. Chem. Soc.*, 2008, **130**, 3023–3029.

19 Q. Liu, H. Yu, X. Zhang and Z. Zhang, *J. Mol. Struct.*, 1999, **478**, 23–27.

20 N. M. D. Brown, D. B. Hewitt and B. J. Meenan, *Surf. Interface Anal.*, 1992, **18**, 187–198.

21 Y. Tian, D. Chen and X. Jiao, *Chem. Mater.*, 2006, **18**, 6088–6090.

22 L. Zhu, X. Liu, J. Meng and X. Cao, *Cryst. Growth Des.*, 2007, **7**, 2505–2511.

23 R. X. Yan and Y. D. Li, *Adv. Funct. Mater.*, 2005, **15**, 763–770.

24 (*a*) G. Jia, H. You, Y. Song, Y. Huang, M. Yang and H. Zhang, *Inorg. Chem.*, 2010, **49**, 7721–7725; (*b*) J. Yang, Z. Quan, E. Kong, X. Liu and J. Lin, *Cryst. Growth Des.*, 2007, **7**, 730–735.

25 (*a*) B. R. Judd, *Phys. Rev.*, 1962, **127**, 750–761; (*b*) H. Mai, Y. Zhang, R. Si, Z. Yan, L. Sun, L. You and C. Yan, *J. Am. Chem. Soc.*, 2006, **128**, 6426–6436.

26 R. L. Booker, *J. Opt. Soc. Am.*, 1981, **71**, 139–144.

27 (*a*) Q. Ju, D. Tu, Y. Liu, R. Li, H. Zhu, J. Chen, Z. Chen, M. Huang and X. Chen, *J. Am. Chem. Soc.*, 2012, **134**, 1323–1330; (*b*) H. B. Na and T. Hyeon, *J. Mater. Chem.*, 2009, **19**, 6267–6273; (*c*) H. B. Na, I. C. Song and T. Hyeon, *Adv. Mater.*, 2009, **21**, 2133–2148; (*d*) J. Y. Park, M. J. Baek, E. S. Choi, S. Woo, J. H. Kim, T. J. Kim, J. C. Jung, K. S. Chae, Y. Chang and G. H. Lee, *ACS Nano*, 2009, **3**, 3663–3669; (*e*) H. Hifumi, S. Yamaoka, A. Tanimoto, T. Akatsu, Y. Shindo, A. Honda, D. Citterio, K. Oka, S. Kuribayashi and K. Suzuki, *J. Mater. Chem.*, 2009, **19**, 6393–6399; (*f*) J. L. Bridot, A. C. Faure, S. Laurent, C. Riviere, C. Billotey, B. Hiba, M. Janier, V. Josserand, J. L. Coll, L. Vander Elst, R. Muller, S. Roux, P. Perriat and O. Tillement, *J. Am. Chem. Soc.*, 2007, **129**, 5076–5084.

28 M. Bottrill, L. K. Nicholas and N. J. Long, *Chem. Soc. Rev.*, 2006, **35**, 557–571.

